

# Finite Element Simulation of Deployment of Large-Scale Confined Inflatable Structures

Eduardo M. Sosa<sup>1\*</sup>, Jerry Choo-Siang Wong<sup>1</sup>, Adi Adumitroaie<sup>2</sup>,  
Ever J. Barbero<sup>1</sup>, Gregory J. Thompson<sup>1</sup>

<sup>1</sup> Department of Mechanical and Aerospace Engineering, West Virginia University, Morgantown, WV 26506-6106, USA

<sup>2</sup> Institute of Constructional Lightweight Design, Johannes Kepler University Linz, Linz-Donau 4040, Austria

\*Corresponding Author: e-mail: [eduardo.sosa@mail.wvu.edu](mailto:eduardo.sosa@mail.wvu.edu)

## Abstract

Large-scale inflatable structures have become a viable alternative for sealing and isolating segments of large-diameter conduits or tunnel sections to prevent the propagation of flooding, noxious gasses or smoke. In such applications, the inflatable structure is prepared for placement, either permanently or temporary, and left ready for deployment, inflation, and pressurization when needed. Once deployed and in operation, the level of sealing effectiveness depends on the ability of the inflatable structure to deploy and self-accommodate, without human intervention, to the intricacies of the perimeter of the conduit being sealed. This work presents finite element evaluations of the deployment and inflation of a full-scale inflatable plug placed within a tunnel section. Folding sequences and controlled deployment techniques developed experimentally served as the basis for the development of finite element models that can simulate different stages of folding, placement, initial deployment and full inflation of the structure. The good level of correlation between experimental and simulation results in terms of deployment dynamics, levels of contact as well as number and position of zones with no contact in the confining perimeter, demonstrate that the proposed modeling strategy can be used as a predicting tool of the behavior of a large-scale inflatable structure for a given confining environment.

**Keywords:** Confined Inflatable; Conformity; Contact; Deployment; Folding; Modeling; Tunnel.

## 1. Introduction

The protection of underwater and underground assets is of a high priority for transportation and security agencies around the globe. Underwater rail transit tunnels are susceptible to disruptions due to flooding originated by extreme climatic events such as hurricanes or man-made events [1-3]. Some examples of such incidents in the United States include the 1992 Chicago freight tunnel flood which forced the shutdown of the subway system, caused damage to numerous businesses, and required the evacuation of about 250,000 people from the area [4]. In 2003, Hurricane Isabel caused flooding of the Midtown Tunnel in Virginia. During this event, about 167,000 m<sup>3</sup> of water from the Elizabeth River flooded the tunnel system in just 40 minutes. The flooding left the tunnel damaged and closed for nearly a month [5]. Most recently, in New York City, seven subway tunnels under the East River as well as three road tunnels flooded during Hurricane Sandy and remained inoperable for several days [6, 7]. These incidents and others summarized in [2] have demonstrated a need for research on ways to mitigate vulnerabilities or, at least, minimize the consequences of catastrophic events. Although it is impossible to prevent all situations that can lead to flooding, damage can be substantially minimized by reducing the area affected by the threatening event. In order to minimize the effects of any eventual threat, a possible approach is to compartmentalize the tunnel system. However, it can be difficult, if not impossible, to install or repair in an existing tunnel all the elements required for compartmentalization. Typically, space constraints inhibit the installation of new protective devices such as flood gates. The elevated cost of interrupting the tunnel operations or making major infrastructure modifications have also discouraged attempts to improve the tunnel resilience by these means.

In the recent years, alternative solutions have been proposed to seal tunnel segments susceptible to the consequences of extreme events. One type of thin-walled structures are the inflatable structures [8]. In particular, large-scale inflatable structures for protection of civil transportation infrastructure, such as railway tunnels, large pipes or mines, have been under development as reported by Barrie [9], Martinez et al. [10], Fountain [11], Lindstrand [12] and Stocking [13]. The implementation of large-scale inflatable structures (also called inflatable plugs) inside transportation tunnels is intended to prevent or reduce the damage induced by hazardous

events by creating a compartment to contain the threat. Potential threats include flooding, smoke or noxious gasses that can propagate through a tunnel system and compromise its functionality and structural integrity. The inflatable structures can be installed at specific locations of the tunnel in order to create a compartment that can isolate the compromised region [10]. Most recently, Barbero et al. [14, 15] and Sosa et al. [16, 17] reported testing efforts performed at different scales to demonstrate the feasibility of containing flooding with inflatable structures. Under these efforts, multiple tests were performed using specially built testing facilities designed to simulate flooding of a tunnel segment. These tests generated valuable experimental information and provided several lessons for field implementation. However, carrying out this type of tests, especially at the full-scale level, is a complex task in which only a limited number of evaluations can be completed within the limits of the allocated time and resources.

The implementation of large-scale inflatable structures for sealing tunnel segments can be divided into three main phases: I. Preparation and installation of the inflatable; II. Initial deployment and inflation; and III. Pressurization. Phase I requires the definition and implementation of a folding pattern in conjunction with packing of the folded plug in a storage container. This phase also includes the transportation and installation of the folded plug at specific locations inside the tunnel system, leaving it ready to be activated when needed. Phase II begins with the detection of a threatening event, which triggers automatic opening of the storage container allowing the liberation of the inflatable followed by inflation until it reaches its final shape and position for isolating specific tunnel segments. When the plug is fully inflated and in place, Phase III starts with the pressurization process for maintaining the plug in position, predominantly by friction, while it withstands the external pressure originated by flooding or gases [10, 14-17].

Full-scale tests corresponding to Phase III showed that the sealing capacity of the pressurized inflatable is a function of the level of local and global conformity achieved during Phase II. Moreover, full-scale tests of Phases I and II demonstrated that it can take several iterations to achieve satisfactory results that cannot be predicted in advance [15, 16]. Consequently, the development of simulation models based on finite element analysis became imperative to have a predicting tool that can anticipate the performance of the inflatable during the different phases of

implementation and operation. As such, this work focuses on the simulation work developed for Phases I and II outlined previously.

An overview of full-scale experimental work that served as a reference for the development of finite element (FE) is presented first, including key features that were implemented later in the development of the FE simulations. The modeling approach and a description of relevant components of the FE models are introduced next, followed by simulation results and comparison of the level of correlation with experimental results. Significant observations and conclusions are presented at the end.

## **2. Overview of Experimental Investigation**

### ***2.1. Inflatable Plug***

The full-scale prototype manufactured for testing purposes consists of a cylindrical segment closed by two hemispherical end caps. The design of the inflatable plug for sealing a tunnel section is based on the procedure outlined by Barbero et al. [14]. The cylinder has a diameter of 4.940 meters and a length of 4.641 meters. The radius of each hemispherical end cap is 2.469 meters, and the total plug length is 9.581 meters. The length of the cylindrical segment was determined based on friction tests run at the coupon level on samples of membrane materials and validated by small-scale prototypes subjected to induced slippage [17]. The perimeter of the cylindrical portion was designed to cover elements that typically exist in a tunnel segment, such as duct-banks, pipes, cables, and rails. However, a manufacturing oversizing of 5% was added to the nominal perimeter to ensure maximum contact of the plug membrane with the tunnel perimeter. The length of the cylindrical portion of the plug provides sufficient contact length for the development of frictional forces to maintain the axial stability, while the circumferential perimeter of the cylinder ensures local conformity of the plug to the tunnel inner perimeter.

The membrane of the inflatable plug consists of a three-layer system comprised of an internal bladder, an intermediate protective fabric, and an external macro-fabric. The bladder is the innermost layer of the construction and is in direct contact with the fluid used for inflation and pressurization. The function of the intermediate fabric restraint is to protect the inner bladder. The

outermost layer is a macro-fabric comprised of woven webbings following a plain weave pattern. The webbings of the macro-fabric are 5-cm wide, 3-mm thick and are manufactured with Vectran fibers [18]. Structurally, the outermost layer is the most important since it carries the membrane stresses generated by the pressurization while the two inner layers provide watertightness and contribute to the total mass and volume of the membrane. Two metallic fittings for inflation and air-release are also integrated into the membrane of one of the hemispherical end caps. The total weight of the inflatable plug including inflation fittings is approximately 907 kg. An overview of the inflatable plug during an unconfined inflation is illustrated in Figure 1(a).

## ***2.2. Folding and Packing***

In aerospace applications, inflatables are typically folded following two main patterns. One of the simplest folding patterns is the “z-fold” in which the inflatable is flattened before being simply folded back and forth at regularly spaced intervals at discrete lines or hinges. However, despite the simplicity, the discrete nature of the folding creates a discontinuous structure that, during the inflation, restricts the airflow between sections and results in a structure that is sensitive to small changes in shape with an unpredictable and dynamically unstable deployment path [19, 20]. The other common folding pattern is by rolling or coiling the deflated structure. This is an effective and compact method to fold and pack an inflatable structure with minimal residual creases. Depending on the configuration, rolling can be in a single or multiple directions. For this folding method it is common to implement passive controls or retardation devices, such as coil springs, Velcro strips or tie-downs installed to produce a more predictable deployment by controlling the final unrolling velocity and minimizing sudden release of sections. This technique results in a more controlled deployment that tends to be much more stable dynamically [19].

In this work, a combination of folding by rolling and installation of passive controls was implemented experimentally and later reproduced in the FE simulations. A sequence of preparation steps was developed for packing the deflated plug inside a portable container that was later placed inside a mockup tunnel section specially built for full-scale tests. These steps were designed to systematize the preparation process so it can be repeated consistently and for maximizing the

contact between the membrane and elements installed on the perimeter of tunnel inner perimeter. The maximization of contact was achieved by minimizing the formation of gaps in sensitive areas such as corners and changes of direction in the profile that will later reduce the sealing effectiveness of the inflatable [15, 16]. The folding and packing sequences developed experimentally were driven by the dimensions and the weight of the inflatable as well as the need for controlled distribution and release of membrane material during the inflation process. Unlike in inflatables of aerospace applications where gravity is at a reduced level from that on Earth, gravity plays a more important role on how the inflatable deploys and how it finally positions within the tunnel section in this application.

Following the sequence depicted in Figure 1, the folding and packing process implemented experimentally included: (a) unconstrained inflation for repositioning reference lines and surface inspection; (b) controlled deflation and beginning of the folding process of the hemispherical end caps; (c) flattening, attachment to the portable container and beginning of folding sequence of cylindrical portion of the plug; (d) creation of longitudinal crease to control the release of membrane material by the installation of tie-downs along the cylindrical portion of the inflatable; (e-f) folding by rolling following longitudinal reference lines pre-marked on the cylindrical portion of the inflatable; (g) final packing of folded plug into the container and closure of vertical soft-cover; (h) transportation and securing the container into the tunnel mockup; and (i) final positioning of the container on the sidewall of the tunnel mockup. Once steps (a) to (i) are completed, the folded plug is ready for a deployment and inflation test.

### ***2.3. Test Setup***

The testing facility built for full-scale tests consists of a tunnel segment to replicate a typical rail tunnel section. The tunnel segment is 15 meters long and 5 meters in diameter. The interior of the tunnel segment (Figure 1(i)) has a profile and typical features that can be found in an actual rail tunnel. The inflation system is designed to operate with air during the initial inflation and then with water during full pressurization of the inflatable for flooding simulations [15-16]. Considering that this work is mainly focused on the initial deployment and inflation with air at a pressure lower

than 2 kPag, only the main components relevant to this operation are outlined here. The inflation of the plug required a low-pressure, high-flow air fan connected to the inflation port of the plug by a set of rigid and flexible hoses. The airflow rate was measured with laminar flow element (LFE) installed in the pipeline. The air blower was also connected to an automatic control system that regulated the flow rate and monitored inflation pressure in the inflatable. Figure 1(j) shows a schematic of the arrangement of the main components of the air inflation system.

#### **2.4. Test Results: Deployment and Inflation**

The deployment of the plug started with the automatic activation of the opening mechanism installed in the vertical soft-cover of the container. The immediate loosening of the laces holding the segments of the soft-cover released the pretension and liberated the folded plug which started to unroll by its own weight and then gradually moved out of the container as the air inflation began. The air inflation process consisted of two stages: 1) Initial inflation at a constant airflow rate of  $0.7 \text{ m}^3/\text{sec}$  until the plug is fully inflated and positioned in the tunnel section; and 2) Once the plug was fully inflated, the air flow was reduced to  $0.023 \text{ m}^3/\text{sec}$  and the internal pressure was kept constant at 1.7 kPag. With this test configuration, the total time from initial deployment to full inflation averaged 180 seconds. Figure 2 shows an example of the inflation sequence including the initial unfolding ( $0 < t < 10$  seconds), inflation ( $10 < t < 130$  seconds), release of membrane material to cover the ceiling of the tunnel section and final position in the tunnel ( $130 < t < 180$  seconds). The process outlined in Section 2.2, along with the results outlined in this section, served as a reference for the development of the FE models presented next.

### **3. Finite Element Simulation**

#### **3.1. Modeling approach and modeling tools**

The execution of the tests described in the previous section took several iterations to achieve consistent results that could not be predicted in advance. So the development of FE simulations to generate a predicting tool that can anticipate the performance of the inflatable became essential. The FE models were developed to increase the understanding of the deployment and inflation

dynamics as well as for the evaluation of the interaction of the inflatable with the confining surface of the tunnel.

The development of an FE model able to reproduce the work performed experimentally required the creation of several components that constituted the whole model. The two main components are the inflatable plug, and a tunnel segment in which the folded plug will be installed, and that will provide the confining environment during the inflation. Additional components created for the modeling process included auxiliary surfaces that helped to replicate the folding procedures implemented in the full-scale prototype. Both main and auxiliary components of the FE model were generated using the Simulia/Abaqus simulation suite [21] and Altair's Hypermesh [22]. The models were solved using the explicit time integration scheme available in Abaqus/Explicit [21]. Hypermesh was used before solving the models to correct element distortions preventing drastic reduction of stable time increments used in the explicit scheme or even a premature analysis termination.

### ***3.2. Geometry and Mesh***

The inflatable plug shown in Figure 3(a) served as the basis for the creation of the first main component of the FE model. Figure 3(b) shows the CAD/CAE model including the geometry partitions of the inflatable created with the purpose of bounding the position of inflation ports, internal chamber surfaces, folding surfaces and folding lines located on the cylindrical segment of the inflatable. Figure 3(c) shows the final meshed configuration of the inflatable. As mentioned in section 2.1, the membrane of the inflatable plug consists of a three-layer system comprised of an internal bladder, an intermediate protective fabric, and an external macro-fabric. The bladder is the innermost layer of the construction and is in direct contact with the fluid used for inflation and pressurization. The function of the intermediate protective fabric is to shield the inner bladder. Both, the internal bladder and the intermediate protective fabric are oversized 5% with respect to the external macro-fabric. The purpose of having oversized inner layers is to prevent them carrying membrane stresses originated by the pressurization. Conversely, the outermost layer consisting of a macro-fabric comprised of woven webbings is designed to carry the membrane stresses.

Structurally, the outermost layer is the most important since it carries the membrane stresses generated by the pressurization while the two inner layers only provide water tightness. Moreover, the two inner layers contribute to the total mass and volume of the whole membrane. With these considerations, the three-layered membrane of the testing prototype was modeled with an equivalent single-layer membrane built from M3D3 membrane elements with an equivalent thickness of 7.7 mm. About 91% of the equivalent thickness corresponds to the macro-fabric, and the remaining 9% corresponds to the two inner layers.

The model of the inflatable plug also includes two metallic fixtures used as air fill and air release ports. These two fixtures are located over one of the hemispherical end caps as shown in Figure 3(b). Since these fixtures are much more rigid than the structural membrane, they are modeled with R3D4 rigid elements.

The second main component of the FE model is the tunnel segment. In this study, the tunnel segment is assumed to be a non-deformable rigid body and therefore modeled with R3D4 rigid elements. The dimensions and features of the tunnel profile shown in Figure 1(i) were used as a basis for the creation of the CAD/CAE models illustrated in Figure 4. The remaining auxiliary components of the model included a flat base and rotational plates created for aiding during the simulation of the folding process. Similarly to the model of the tunnel segment, these surfaces were considered non-deformable and were created with R3D4 rigid elements.

### ***3.3. Material Properties***

The fabric material model available in Abaqus was implemented to represent the mechanical properties of the equivalent single-layer membrane. Since the strength of the equivalent single-layer membrane is dominated by the macro-fabric created by the woven webbings, the constitutive relationship in the fill and warp directions of the macro-fabric was derived from reduced-scale elongation tests [17]. In these tests the macro-fabric displayed a linear behavior with a tensile strength of 258 MPa in both warp and fill directions for a maximum strain 0.1. Moreover, the in-plane shear stiffness of the macro-fabric was included the material model according to the results obtained from picture frame tests performed with woven webbings [23]. In the model, an artificial

compression strength of 10% of the tensile strength for a maximum strain of -0.1 was added to avoid the collapse of wrinkled elements under compressive loading when the plug is deflated [21].

The total mass of the inflatable plug including the inflation fixtures is 907 kg. A static friction coefficient 0.19 was used between the external surface of the membrane and the tunnel inner surface. A static self-friction coefficient of 0.21 was used for the fabric-to-fabric friction. These two values were obtained from experimental evaluations at coupon level and from reduced-scale experiments [17]. These two friction values define how the surface of the membrane interacts with itself and the tunnel surface as the deployment and inflation develop during the simulation. The tie-downs installed in the experimental evaluations for sequential membrane release were represented by uniaxial connector elements with a nominal breaking capacity of 0.8 kN for a breaking elongation of 20 mm.

### ***3.4. Folding and Placement***

The simulation of the folding process was implemented as a set of geometric transformations comprised of a combination of rigid body rotations and translations applied as boundary conditions to selected sets of nodes and elements previously marked on the surface of the inflatable. The main purpose of the geometric transformations was to emulate the actual folding sequence illustrated in Figure 1. Folding lines were created from sets of nodes positioned on the surface of the cylindrical portion of the inflatable that guided the folding process.

As in the experimental work, the simulation of the folding process included the following general steps: 1) unconstrained inflation; 2) flattening; and 3) folding by successive rolling. In the first step of the simulation, the starting position of the inflatable is in unconstrained and unstressed conditions and using the nominal design geometry. In the second step, the deflation is achieved by vertical gravity force, and small horizontal displacements applied to the cylindrical portion of the inflatable. Both are applied simultaneously to initiate the flattening process as illustrated in the sequence of Figure 5 leading to Figure 6. Once the inflatable is flattened and laying on the base plate, the folding process began by forming a longitudinal crease designed to hold and sequentially release membrane material during the deployment process. At this stage, 15% of the membrane

circumferential perimeter of the cylindrical portion was held by tie-downs placed along the edges of the initial fold placed in the cylindrical portion of the inflatable. In the third step, the folding sequence was implemented by gradual rolling of the flattened membrane by successive lifting and partial rotations of the partial folds by using the auxiliary rotational rigid plates. Three sets of lifting and rotation maneuvers, combined with vertical gravity force were applied to complete the folding sequence. Figure 7 illustrates the sequence of the last set of lifting and rotation maneuvers and the resulting folded configuration of the plug. At this point, the mesh of the folded plug was verified for the purpose of correcting excessive element distortion, interpenetration of elements and other irregularities that would inhibit the solution process in subsequent modeling steps.

After the folding process was complete, the simulation continued with the placement of the folded plug into the storage area of the tunnel section. This process consisted of a combination of a rigid body rotations and translations to approach the folded plug to the tunnel and place it within the storage area depicted in Figure 4(a). Once in place, the folded plug was connected to the tunnel along a predefined horizontal line located inside the storage area that provided anchorage and alignment to the inflatable during the initial deployment and inflation process. The final positioning in the storage area was completed by further horizontal translation as shown in Figure 8(a). At this stage, a second verification of the folded mesh was implemented to restore distorted elements back to their original condition before doing the deployment simulation. In the simulation of folded membranes it is typical to execute a mapping process consisting in passing either node's or element's coordinates from an initial configuration to a reference (or metric) configuration for restoring distorted elements [21]. In the simulation, a rigid plane representing a vertical cover closed the storage area as the restoration of the mesh commenced as shown in the sequence of Figures 8(a) to 8(c). When the storage area was closed, a vertical gravity force was applied to the folded plug as shown in Figure 8(d). The result of mesh restoration and vertical gravity force defined the starting position of the folded plug for the simulation of deployment and inflation.

### **3.5. Initial Conditions**

The folded plug placed in the storage area illustrated in Figure 8(d) was the starting

configuration for simulation of deployment. In this configuration, the folded plug sits on the base of the storage area under the effect of its weight. A vertical cover and container surfaces holds it up until the deployment sequence is activated. In Figure 8(d), the folded plug is connected to the tunnel section along a single line B. The nodes along line B have only rotational degrees of freedom. This boundary condition represents the ties that fasten and restrain the inflatable plug to the tunnel section and are assumed to be unbreakable during the deployment simulation. The tunnel section is assumed to be a rigid body fixed in X, Y, and Z directions.

In the modeling of folded membranes initial errors and mesh distortions are introduced inevitably during the folding process. These distortions in the folded mesh may lead to initial stresses that can affect the final shape of the deployed inflatable structure by creating fictitious wrinkles or bogus stress concentrations that do not exist in the real structure. The reference configuration illustrated in Figure 3(c) was maintained active during the deployment simulation to define the unfolded stress-free configuration of the inflatable plug. Under this procedure, as the reference configuration is specified for all the membrane elements, any initial stress conditions specified for the same element are ignored, therefore no initial stresses were included in the membrane of the folded plug [20]. Maintaining the reference configuration active also contributed to stabilizing the simulation process and avoid distortions on the membrane surface when the inflatable is fully positioned in the tunnel segment.

### ***3.6. Inflation Method***

The Uniform Pressure Method (UPM) originally proposed by Wang and Nefske [24], and currently available in Abaqus/Explicit [21], was implemented in this work for simulation of the inflation process. The UPM method has been widely implemented for more than two decades in the simulation of automobile airbag inflation [25-31], also in inflatables used in the aerospace industry [32-35] and more recently, in the evaluation of deflation of large-scale air inflated arch frames [36]. For the purposes of this work, the UPM method was found to be adequate for simulating a relatively slow inflation, since the inertia of the inflation gas can be neglected, at a reasonable computational cost. The implementation of more sophisticated algorithms, such as the

Coupled Eulerian Lagrangian (CEL) method [30] and the Arbitrary Lagrangian Eulerian (ALE), or mesh-free methods, such as the Smoothed Particle Hydrodynamics (SPH) or the Finite Pointset Method (FPM) [21, 37-38], was ruled out at this stage primarily because of their elevated computational cost (in the order of about 4 to 15 times higher than UPM depending on the mesh density) and the difficulty of obtaining and calibrating all the necessary parameters to build an accurate model within a reasonable time.

The main assumption of the UPM is that the pressure within the inflatable is spatially uniform during the inflation [24]. A combination of multi-chamber and fluid exchange approaches were implemented to extend the capability of the UPM to better replicate the actual deployment behavior observed during the experiments at full-scale. The UPM available in Abaqus/Explicit required the definition of surface-based cavities to model the fluid-structure interaction during the inflation process [21]. This capability allowed to use standard finite elements to model the membrane of the inflatable, but also required a surface definition on the cavity boundary for coupling the deformation of the membrane and the pressure exerted by the inflation fluid. Moreover, the UPM required the definition of the fluid behavior as well as the fluid exchange sequence to model the flow of the fluid. The method also required the definition of the properties of an inflator for modeling the inflation of the cavities.

Most of the pre-simulation conditions for modeling of a confined inflatable are similar to those typically applied to simulations of automobile airbags. However, additional considerations were taken into account to define specific conditions for the simulation of a large-scale confined inflatable structure. The following additional conditions were implemented to account for the particularities of the problem at hand, including: a) Vertical gravity force is applied on the entire inflatable plug from the beginning to the end of the inflation simulation; b) The ambient surrounding the plug is air at a temperature of 27°C and standard ambient pressure; c) The inflator provides an airflow rate of 0.7 m<sup>3</sup>/sec and the total inflation time is 180 seconds. Both values are based on experimental results [15-16], however, the total analysis time was extended to 200 seconds; d) The air inflow behaves as an ideal gas with constant fluid temperature (isothermal process); e) The air is assumed to be transferred into and within the inflatable through an orifice

with a discharge coefficient of 1.0; f) The air used for inflation enters into the plug through one of the inflation fixtures located on the hemispherical end cap; g) The membrane representative the actual structural fabric is assumed to be impermeable; and h) The walls of the internal chambers generated to direct the airflow inside the inflatable do not contribute to the mass or structural capacity of the external membrane. The position of the internal chambers delimited by chamber walls placed inside the inflatable is illustrated in Figure 9.

### ***3.7. Model Configurations***

Three models were generated to simulate initial deployment and inflation including the conditions and properties outlined previously. In Deployment #1 (D1), the folded plug did not include tie-downs to control the release of membrane material; moreover, the air flow was not directed within the plug, that is, the airflow started filling up the entire plug evenly once it entered into Chamber 2, as illustrated in the sequence of Figure 9(a). In Deployment #2 (D2), the folded plug included tie-downs modeled with connector elements that were installed during the folding process. Similarly to D1, the air flow was not directed within the plug. 3) In Deployment #3 (D3) the folded plug also included connector elements installed during the folding process. Model D3 included a sequence of fluid exchange designed to guide the airflow within the plug as illustrated in the sequence of Figure 9(b), where the airflow enters into Chamber 2, then fills up the first half (from Chamber 1 to Chamber 3) immediately after entering into the plug. After this initial step, which takes one-tenth of the total inflation time, the second half (Chamber 4) of the plug starts inflating. For all these three modeling configurations, the evolution of the total membrane area, the inflated volume, the inflation pressure and the total contact area were computed for analysis of the inflation process.

### ***3.8. FE Results and Discussion***

Since the FE models were developed to mimic the experimental work, the simulation results are compared with available experimental data corresponding to the initial deployment and inflation of the plug. Upon removal of the vertical cover, the plug starts to unroll out of the storage

area initiating the deployment process. This initial step is illustrated in the sequence of Figure 10 where the folded plug falls by its weight first onto the side step of the tunnel profile, and then rolls out towards the tunnel floor. The initial unroll takes around 2.4 seconds and the model reproduced reasonably well the sequence observed experimentally. This initial movement was common for all three deployment models (D1 to D3).

Immediately upon completion of the initial unroll, the inflator is activated initiating the inflation process. Figure 11 illustrates the inflation process as a sequence of images captured from full-scale experiments compared to the results predicted by models D1, D2, and D3. The total analysis time is  $t_T = 200$  seconds and the accumulated time  $t$  corresponding to each image is normalized with respect to  $t_T$ , then, the normalized time is defined by  $t_n = t / t_T$ .

In Figure 11, using the normalized time as a reference, models D1 and D2 show a similar inflation pattern from  $t_n = 0.05$  to  $0.125$ . In these two models, the airflow was not guided within the plug, so the airflow started to fill uniformly once the inflator was activated. The effect of guiding the airflow within the plug showed up in model D3 at  $t_n = 0.125$ , in which the internal chambers closer to the inflation port started filling first before transferring the airflow to the remaining chambers following the scheme illustrated in Figure 9(b).

From  $t_n = 0.275$  to  $t_n = 0.525$ , the retardation effect of including tie-downs in the membrane during the folding process started to show up. Since the membrane of model D1 is not restrained by tie-downs, the upper portion of the plug started to take a cylindrical shape. In models D2 and D3, the combination of guided internal airflow with the presence of tie-downs restraining a portion of the membrane changed the shape of the cylindrical portion of the plug as the inflation progressed. Particularly in model D2, the cylindrical portion contains two lobes separated by the crease created during the folding similar to what was seen during the experimental evaluations. In model D3, the effect of delaying the release of the membrane is combined with the guided airflow as the container side of the plug is inflated first resulting in a shape similar to the one seen in model D1. A closer view of the restraining effect of the tie-downs in the membrane during the inflation is depicted in Figure 12, which compares side by side images captured from one of the full-scale experiments and the inflation model D2 at  $t_n = 0.525$ .

At  $t_n = 0.65$  all models reached nearly three-quarters of the tunnel height. Models D2 and D3 displayed similar shapes with the tie-downs holding the membrane unbroken while model D1 continued moving towards the ceiling of the tunnel section. Between  $t_n = 0.725$  and  $t_n = 1.0$ , the inflatable finally touches the ceiling of the tunnel. In models D2 and D3, the tie-downs holding the membrane broke down between  $t_n = 0.77$  and  $t_n = 0.775$  liberating the portion of the membrane stored between the tie-downs that covered the upper portion of the tunnel section. Finally, at  $t_n = 1.0$ , the plug is fully inflated, and all models have reached their final shape within the tunnel section.

Looking at all the simulation results in comparison with the experimental results of Figure 11 and Figure 12, model D2 seems to follow more closely the inflation pattern observed in the experimental evaluations. Moreover, all simulation models reached an apparent similar final shape at the end of the inflation. Additional post-processing and further analysis of the simulation results allowed a better understanding of the dynamics of the inflation process under confined conditions as well as the levels of conformity and global contact corresponding to each model.

Figure 13 and Figure 14 show, respectively, a series of transversal and longitudinal cross-sections of the inflatable captured during the inflation process. There are three main features of the models that Figures 13 and 14 are capturing to understand the dynamics of the inflation process. The first one is the effect of guiding the flow within the inflatable. This effect is illustrated in Figure 13 for  $t_n = 0.125$ , in which models D1 and D2 show similar shapes indicating the presence of a uniform airflow in the whole inflatable. On the other side, the shape of model D3 indicates that only the storage side of the inflatable is initially receiving airflow while the rest of the membrane remained deflated, as specified in the scheme in Figure 9(b). The second feature captured by the cross-sections is the membrane distribution at the different stages of the inflation. Following to the initial unroll and due to the gravity effect, practically all the membrane material is initially accumulated on the tunnel floor. As the inflation progresses, the membrane material moves from the storage side to the opposite wall and the pressure generated by the airflow lift the membrane so it can gradually climb to the upper portion of the tunnel section. The inflation pressure also contributes to stretch longitudinal and transverse wrinkles by gradually dispersing the membrane material accumulated on the tunnel floor. The membrane distribution as the inflation

progressed is seen for  $t_n = 0.25$  to  $t_n = 1.0$  in the transversal and longitudinal cross-sections of Figure 13 and Figure 14, respectively.

The third feature observed in the cross-sections is the effect of having membrane material held by tie-downs for a determined period during the inflation process. In model D1, the membrane material is driven to the upper portion of the tunnel by the inflation pressure. However, the friction between the membrane and the tunnel wall does not allow to get sufficient membrane material to cover properly all the intricacies of the upper area of the tunnel section. The consequence of having this effect is the lack of local conformity manifested by the presence of local gaps and the accumulation of longitudinal wrinkles on the floor or lateral walls as illustrated in Figures 13 and 14 for  $t_n = 0.77$  to  $t_n = 1.0$ . On the other hand, models D2 and D3 showed a better material distribution and a better final coverage when the membrane was temporarily held and strategically released in the upper tunnel transition areas. This is illustrated in both Figures 13 and 14 during the inflation progress until the tie-downs break at  $t_n = 0.77$ . Since the pressure generated by the airflow continues being applied, it lifts the recently released membrane from  $t_n = 0.775$  to  $t_n = 1.0$ . Clearly the inclusion of tie-downs for temporarily holding off the membrane fulfilled two purposes during the inflation process: a) reserve membrane material for coverage of selected zones, in this case the upper portion of the tunnel section, and, b) reduce the formation of longitudinal wrinkles in the lower areas of the tunnel at the end of the inflation, as illustrated in Figures 13 and 14. The result of this desired behavior is improved local conformity revealed by no gaps in the contact perimeter, which translates in an increased sealing capacity of the inflatable plug. All these observations are also consistent with the observations made during the full-scale experimental work [15-16].

Figure 15 shows an interior view of the position of longitudinal wrinkles at the end of the inflation corresponding to model D3 in comparison with experimental observations. As seen in Figure 15, the position and extension of major wrinkles are in very good agreement with the image captured from experimental results. As noted previously, the presence of longitudinal wrinkles is related to how the membrane material is driven during the inflation, but it is also function of the percentage of the oversizing of the perimeter of the cylindrical portion of the plug. The extra

membrane material added for manufacturing process intends to account for unforeseen elements in the tunnel that can increase the total perimeter to be sealed. It also accounts for the non-uniform nature of the deployment process that can lead to an irregular distribution of membrane material during the initial inflation. Under normal operating conditions and no major disturbances, the extra membrane material would not be needed and, therefore, will also contribute to the formation of longitudinal wrinkles.

The level of local conformity is illustrated in Figure 16, which shows a series of close-up views of the local conformity obtained from experimental results in comparison with simulation results. The most critical areas in terms of local conformity are the corners and transitions along the contact perimeter. Also, from Figure 13 at  $t_n = 1.0$ , it is seen that model D1 showed at least three visible gaps around the perimeter while models D2 and D3 did not show evident gaps other than those associated with the local membrane FE mesh density at corners or transitions as illustrated in the close-up views of Figure 16.

The evolution of selected numerical outputs obtained from the different models is presented in Figure 17. The evolution of the total membrane surface area, as the inflation progressed, is illustrated in Figure 17(a). This graph shows the ability of the inflation model to restore the reference configuration and to reach the membrane area calculated for unconfined conditions at a pressure of 1.72 kPag. This level of pressure is only about  $1/70^{\text{th}}$  of the operational pressure required during flooding simulations [15-16]. The membrane area was calculated to verify that the membrane of the inflatable is not over stretched and with an elongation compatible with the material model. Figure 17(a) shows that all three models displayed a similar evolution pattern until reaching the ideal area of  $\sim 150 \text{ m}^2$  calculated for unconfined conditions. A summary of the final membrane areas computed for all the models at the end of the total analysis time is summarized in Table 1.

Figure 17(b) shows the evolution of the plug inflated volume as the inflation progressed. The volume of model D1 increased smoothly while models D2 and D3 showed a sudden increase in the volume at  $t_n = 0.775$ , consistent with the membrane release upon breakage of the restraining tie-downs. However, the confinement effect of the tunnel does not allow the inflatable reaching

the total volume calculated for unconfined conditions. All three models reached about 85% of ideal unconfined volume. The main effect of not reaching the total volume corresponding to the unconfined inflation is the formation of longitudinal wrinkles as illustrated in the longitudinal cross sections of Figure 14 and Figure 15.

The evolution of inflation pressure for models D1 to D3 in comparison with experimental results is illustrated in Figure 17(c). These results indicate that the inflation pressure for the different models generally followed the trend observed experimentally with relatively small fluctuations as the plug unrolled during the period of  $t_n = 0$  to  $t_n = 0.5$ , and with a steady increase and a single drop of pressure between  $t_n = 0.5$  and  $t_n = 0.75$ . In the case of the experimental curve, the peaks seen between  $t_n = 0.5$  and  $t_n = 0.75$ , correspond to successive breakage of the tie-downs, which gradually increased the plug volume and temporarily reduced the internal pressure, whereas in models D2 and D3, the breakage of tie-downs was simultaneous, i.e. the tensile strength of the tie-downs was reached in all the ties at the same time. It is worthy to mention that in the experiments, the time of breakage of the tie-downs is defined by the number of ties installed during the folding process described in Section 2.2 and their individual tensile strength. In the execution of the experiments, a crease was created in the membrane by joining equidistant discrete points along lines L1 and L2 located in the cylindrical portion of the inflatable, as illustrated in Figure 1(d). Specifically, ten points located along lines L1 and L2 were joined by using ten tie-downs with a nominal individual tensile strength of 800 N and spaced every 0.4 meters. Reminding that the purpose of using retardation devices is to control the release of the membrane during the inflation process, the inflation pressure defines when those ties will break and release the membrane. In order to maximize the coverage of the membrane in the upper portions of the tunnel section, the release of the membrane stored during the folding process is delayed until the inflatable has reached about 75% of the inflation time. At that point, the inflation pressure originated a total hoop force in the membrane that equals the total force that all the ties can resist before breaking. When the total resisting force provided by the ties equals the total hoop force originated by the inflation pressure, the ties start breaking, and the inflation volume increases as a consequence of the membrane release.

Ideally, a simultaneous breakage of all tie-downs would increase the volume relatively quickly and would produce a single drop in the inflation pressure history. However, tests results showed two or three consecutive peaks suggesting that the intended breakage of the tie-downs was gradual and originated the fluctuations seen in the inflation pressure illustrated in Figure 17(c). In the case of the simulation models D2 and D3, the breakage of all the ties occurred simultaneously which originated a single drop in the pressure around  $t_n = 0.75$  as shown in Figure 17(c). Despite the pressure history predicted by the models does not match exactly the experimental pressure history, the models capture the overall behavior corresponding to the breakage of ties and membrane release.

The evolution of the contact area as the inflation progressed is shown in Figure 17(d). The contact area corresponding to model D1 displayed a relatively steady increase as the inflation progressed while for models D2 and D3 the contact area displayed a sudden increase around  $t_n = 0.775$ . This sudden increase corresponds to the breakage of the tie-downs and the release of the membrane material that covered the ceiling of the tunnel section, thus increasing the contact area. Figure 17(d) also shows the increase in the contact area compared to the ideal contact area corresponding to the cylindrical portion of the inflatable. From this comparison, it is clear that after  $t_n = 0.775$  the contact area surpasses the design contact area. The inflatable plug was designed to have a cylindrical portion with a nominal contact area of  $71.98 \text{ m}^2$  [15-16]. This contact area provides sufficient slippage resistance to hold the external pressure originated from flooding that will try to push the plug along the tunnel section. Looking at the longitudinal cross sections of Figure 14 at the end of the inflation ( $t_n = 1.0$ ), it is clear that the final contact area is higher than the design contact area. The values of contact area at the end of the inflation summarized in Table 1 indicate that the contact area increased 25%, 32%, and 34%, for models D1, D2, and D3, respectively. This increase in the contact area is attributed to the confinement effect of the tunnel section in which part of the hemispherical end caps become part of the cylindrical portion of the plug, thus increasing the total contact area, particularly on the tunnel floor as illustrated in Figure 14 at  $t_n = 1.0$ . However, this apparent increase in the final contact area should be taken with caution. Experimental observations indicated that when the inflatable plug is fully pressurized in

preparation for flooding simulations, the two hemispherical end caps tended to regain their hemispherical shape, and therefore reducing the apparent increase of contact area [15-16]. Finally, the models presented in this work don't account for the texture of the actual macro-fabric comprised of woven webbings without any external coating. This texture leaves small gaps in the contact between the membrane and the surface of the tunnel section that reduce the apparent total contact area. Additional simulation work will be necessary to obtain an estimation of the actual contact area including full pressurization and the texture of the membrane.

#### **4. Conclusions**

This study presented the development of finite element models to simulate the initial deployment and inflation of a large-scale inflatable structure used for sealing a tunnel segment. Simulation models for folding, placement, initial deployment and full inflation were developed, and simulation results were compared with available experimental results obtained from tests with a full-scale prototype.

Simulation results show a good level of correlation with experimental results, particularly in reproducing the overall deployment dynamics consisting of the initial unrolling followed by full inflation of the plug. Moreover, in the simulation cases in which retardation devices were included, the simulation results showed how a controlled release of membrane material during the inflation can lead to improved levels of local conformity and enhanced contact area between the plug surface and the tunnel surface. Considering that the actual contact area is not easily measurable in full-scale experiments, the FE results can provide an estimation of the actual contact area at the end of the low-pressure inflation.

Simulation results also showed that the models can predict the level of conformity, or fit, of the inflatable to the tunnel geometry by identifying gaps in the contact. Lack of local conformity revealed itself in the form of gaps between the inflatable and the tunnel perimeter, particularly in corners, transitions and around obstructions to which the membrane of the inflatable has to adapt in order to seal the tunnel perimeter. The simulation models were also able to reproduce the formation of major longitudinal wrinkles resulting from the excess of membrane material or lack

of uniform distribution around the tunnel perimeter. This information is useful to determine the proper degree of extra membrane material needed in the hoop direction of the cylindrical portion of the plug to maximize the coverage, as well as the need for additional retardation devices to control the distribution or release of membrane material.

Finally, simulation results showed that the implementation of a modeling strategy that includes the application of geometric transformations for folding and positioning of the inflatable, as well as the implementation of the Uniform Pressure Method in combination with retardation devices, provided a reasonably accurate predicting tool. These models allow the development of the further analysis and parametric studies including assessments of the influence of changes in the confining tunnel perimeter, design optimization of the inflatable, alternative folding sequences, alternative ways to guide the air flow within the inflatable plug and the influence of using different airflow rates during the inflation process. Evaluations of variations of all these factors can be very costly at an experimental level. Thus, the availability of a calibrated simulation model contributes to minimization of the need of experimental validations.

### **Acknowledgements**

The authors are grateful to Prof. Christopher Rolinson from the School of Communication at Point Park University for sharing high-definition images captured during experimental tests, some of which were included in this work.

### **References**

- [1] The Blue Ribbon Panel on Bridge and Tunnel Security. Recommendations for Bridge and Tunnel Security. Publication FHWA-IF-03-036. U.S. Department of Transportation, 2003.
- [2] TCRP Report 86/NCHRP Report 525: Public Transportation Security. Volume 12. Making Transportation Tunnels Safe and Secure. Transportation Research Board of the National Academies, Washington, D.C., 2006.

- [3] Rabkin N. Passenger Rail Security, Federal Strategy and Enhanced Coordination Needed to Prioritize and Guide Security Efforts. Publication GAO-07-583T, U.S. Government Accountability Office, 2007.
- [4] Inouye R, Jacobazzi J. The Great Chicago Flood of 1992. *Civil Engineering-ASCE* 1992; 25(62):52–55.
- [5] Post, Buckley, Schuh, and Jernigan. Hurricane Isabel assessment, a review of hurricane evacuation study products and other aspects of the National Hurricane Mitigation and Preparedness Program (NHMPP) in the Context of the Hurricane Isabel Response, National Oceanic Atmospheric Administration (NOAA), March 2005.
- [6] The City of New York. A Stronger, More Resilient New York. URL: <http://www.nyc.gov/html/sirr/html/report/report.shtml>.
- [7] Zimmerman R. Planning restoration of vital infrastructure services following Hurricane Sandy: Lessons learned for energy and transportation. *Journal of Extreme Events* 2014; 1(1) 145004:1-38.
- [8] Godoy LA. *Thin-Walled Structures with Structural Imperfections*. Pergamon, 1996.
- [9] Barrie A. Going Underground: Homeland Security Works on Tool to Prevent Tunnel Disasters. URL:<http://www.foxnews.com/story/0,2933,417461,00.html>.
- [10] Martinez X, Davalos J, Barbero EJ, Sosa EM, Huebsch W, Means K, Banta L, Thompson GJ. Inflatable Plug for Threat Mitigation in Transportation Tunnels. In: *Proceedings of the Society for the Advancement of Material and Process Engineering Conference*, Baltimore, MD, May 21-24, 2012.
- [11] Fountain H. Holding Back Floodwaters with a Balloon. *The New York Times/Science Supplement*. URL: <http://www.nytimes.com/2012/11/20/science/creating-a-balloonlike-plug-to-hold-backfloodwaters.html>.

- [12] Lindstrand Technologies. Inflatable Tunnel Plugs. URL:  
<http://www.lindstrandtech.com/innovation-centre-main/innovation-centre/inflatable-tunnel-plugs>.
- [13] Stocking A. An Inflatable Tunnel Seal Stops Flooding of World's Largest Undeveloped Uranium Mine. URL:  
[http://www.petersenproducts.com/case\\_study/Large\\_Mine\\_Flooding\\_Remediation.aspx](http://www.petersenproducts.com/case_study/Large_Mine_Flooding_Remediation.aspx).
- [14] Barbero EJ, Sosa EM, Martinez X, Gutierrez JM. Reliability Design Methodology for Confined High-Pressure Inflatable Structures. *Engineering Structures* 2013; 51:1-9.
- [15] Barbero EJ, Sosa EM, Thompson GJ. Testing of Full-Scale Confined Inflatable for the Protection of Tunnels. In: *Proceedings of the VI International Conference on Textile Composites and Inflatable Structures, Structural Membranes 2013, Munich, Germany, October 9-11, 2013*.
- [16] Sosa EM, Thompson GJ, Barbero EJ. Testing of full-scale inflatable plug for flood mitigation in tunnels. *Transportation Research Record: Journal of the Transportation Research Board* 2014; 2407, *Structures* 2014, 2:59-67.
- [17] Sosa EM, Thompson GJ, Barbero EJ, Ghosh S, Peil KL. Friction characteristics of confined inflatable structures. *Friction* 2014; 2(4):365–390.
- [18] Kuraray Co. Homeland Security: A Big Plug for Vectran. URL:  
<http://www.vectranfiber.com/NewsInformation/tabid/83/EntryId/23/Homeland-Security-A-Big-Plug-for-Vectran.aspx>.
- [19] Schenk M, Viquerat AD, Seffen KA, Guest SD. Review of inflatable booms for deployable space structures: packing and rigidization, *Journal of Spacecraft and Rockets* 2014; 51(3):762-778.
- [20] Katsumata N, Natori MC, Yamakawa H. Analysis of dynamic behavior of inflatable booms in zigzag and modified zigzag folding patterns, *Acta Astronautica* 2014; 93:45–54.

- [21] Abaqus User's Manual, Documentation Collection Version 6.11, Dassault Systèmes Simulia Corp., Providence, RI.
- [22] Altair HyperWorks User's Manual. Altair Engineering Inc., Troy, MI.
- [23] Peil KL, Barbero EJ, Sosa EM. Experimental evaluation of shear strength of woven webbings. In: Proceedings of the Society for the Advancement of Material and Process Engineering Conference, Baltimore, MD, May 21-24, 2012.
- [24] Wang JT, Nefske DJ. A new CAL3D airbag inflation model. SAE Technical Paper Series 880654. International Congress and Exposition, Detroit, MI, February 29 – March 4, 1988.
- [25] Buijk AJ, Florie CJL. Inflation of folded driver and passenger airbags. In: Proceedings of the MSC World Users Conference, Paper 91-04-B, Los Angeles, California, March 1991.
- [26] Wang JT. An analytical model for an airbag with a hybrid inflator. General Motors Research & Development Center, Crashworthiness and Occupant Protection in Transportation Systems, ASME 1995; AMD-210/BED-30.
- [27] Ha WP, Park SJ, Spit HH. Advanced curtain airbag modeling using the uniform pressure approach combined with a gas flow analysis. SAE 2004; 01-1632.
- [28] Kamiji K, Kawamura N. Study of airbag interference with out of position occupant by the computer simulation. Proceedings of the 17th International Technical Conference on the Enhanced Safety of Vehicles (ESV), Paper #374, Amsterdam, Netherlands, June 4-7, 2001.
- [29] Lee JK, Ha WP, Lee JH, Chae DB, Kim JH. Validation methodology on airbag deployment process of driver side airbag. In: Proceedings of the 21th Enhanced Safety of Vehicles (ESV) Conference, Paper No. 09-0363, Stuttgart, Germany, June 15–18, 2009.
- [30] Simulia. Simulation of airbag deployment using the coupled Eulerian-Lagrangian method in Abaqus/Explicit, Abaqus Technology Brief 2011; TB-11-ABCEL-1.

- [31] Potula SR, Solankia KN, Oglesby DL, Tschopp MA, Bhatia MA. Investigating occupant safety through simulating the interaction between side curtain airbag deployment and an out-of-position occupant. *Accident Analysis and Prevention* 2012; 49:392–403.
- [32] Furey D, Buijk A, Bark LW. Simulation of a helicopter cockpit air bag system with MS/DYTRAN. In: *Proceedings of MSC World Users' Conference*, 1996.
- [33] Salama M, Kuo CP, Lou M. Simulation of deployment dynamics of inflatable structures. *AIAA Journal* 2000; 38(12):2277–2283.
- [34] Wang JT, Johnson AR. Deployment simulation methods for ultra-lightweight inflatable structures. NASA/ TM-2003-212410-ARL-TR-2973.
- [35] Wang JT. Dynamic deployment simulations of inflatable space structures. In: *Proceedings of the 5th International Conference on Computation of Shell and Spatial Structures*, Salzburg, Austria, June 1-4, 2005.
- [36] Lia Q, Guoa X, Qinga Q, Gong J. Dynamic deflation assessment of an air inflated membrane structure. *Thin-Walled Structures* 2015; 94:446-456.
- [37] Hirth A, Haufe A, Olovsson L. Airbag simulation with LS-DYNA, Past-Present-Future. In: *Proceedings of 6th European LS-DYNA Users' Conference* 2007:57-73.
- [38] Graczykowski C. Theoretical models and numerical methods for adaptive inflatable structures. In: *Proceedings of the Fourteenth International Conference on Civil, Structural and Environmental Engineering Computing*, Stirlingshire, Scotland, 2013.

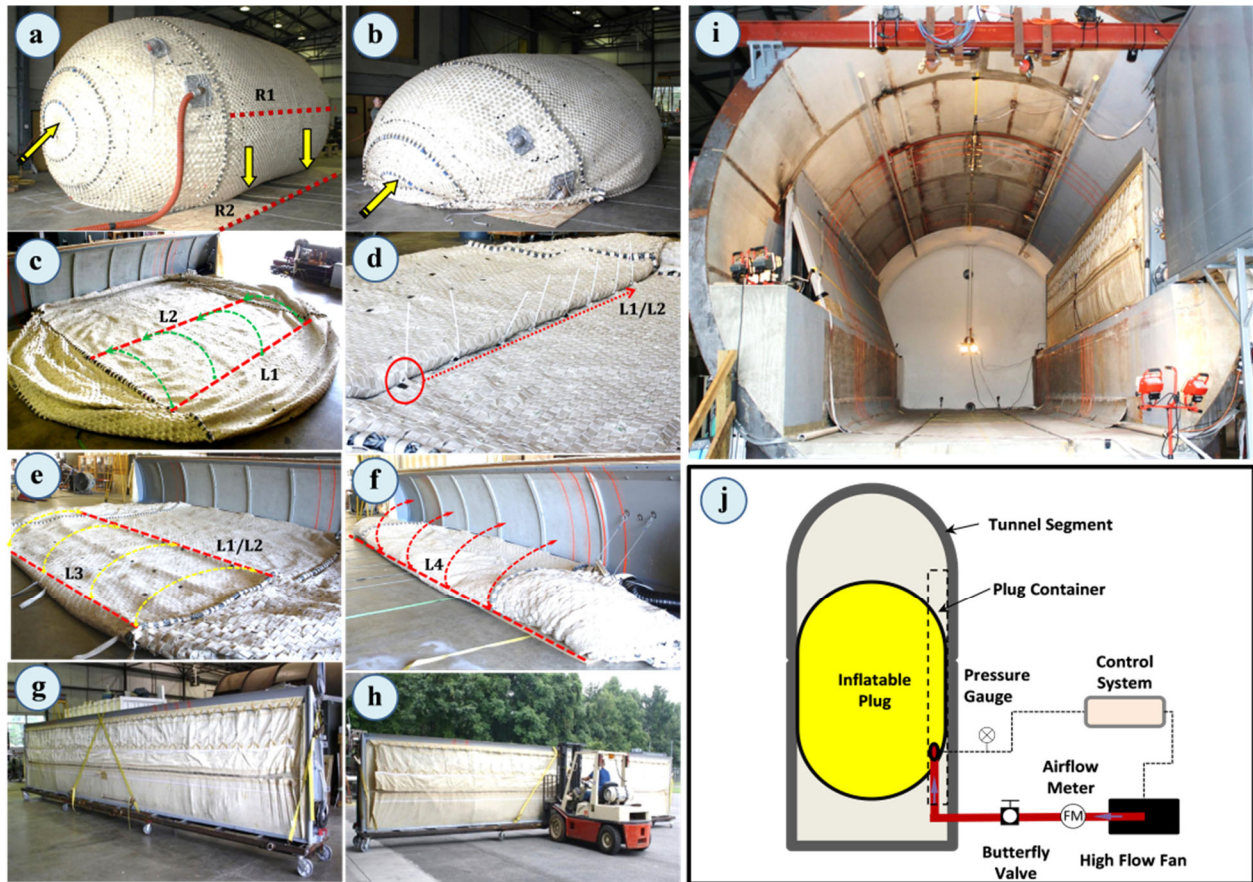


**Figure 1.** (a) to (h) Folding and packing sequence; (i) Interior of tunnel mock-up after installation of portable container; (j) Schematics of test setup for air inflation [15-16].

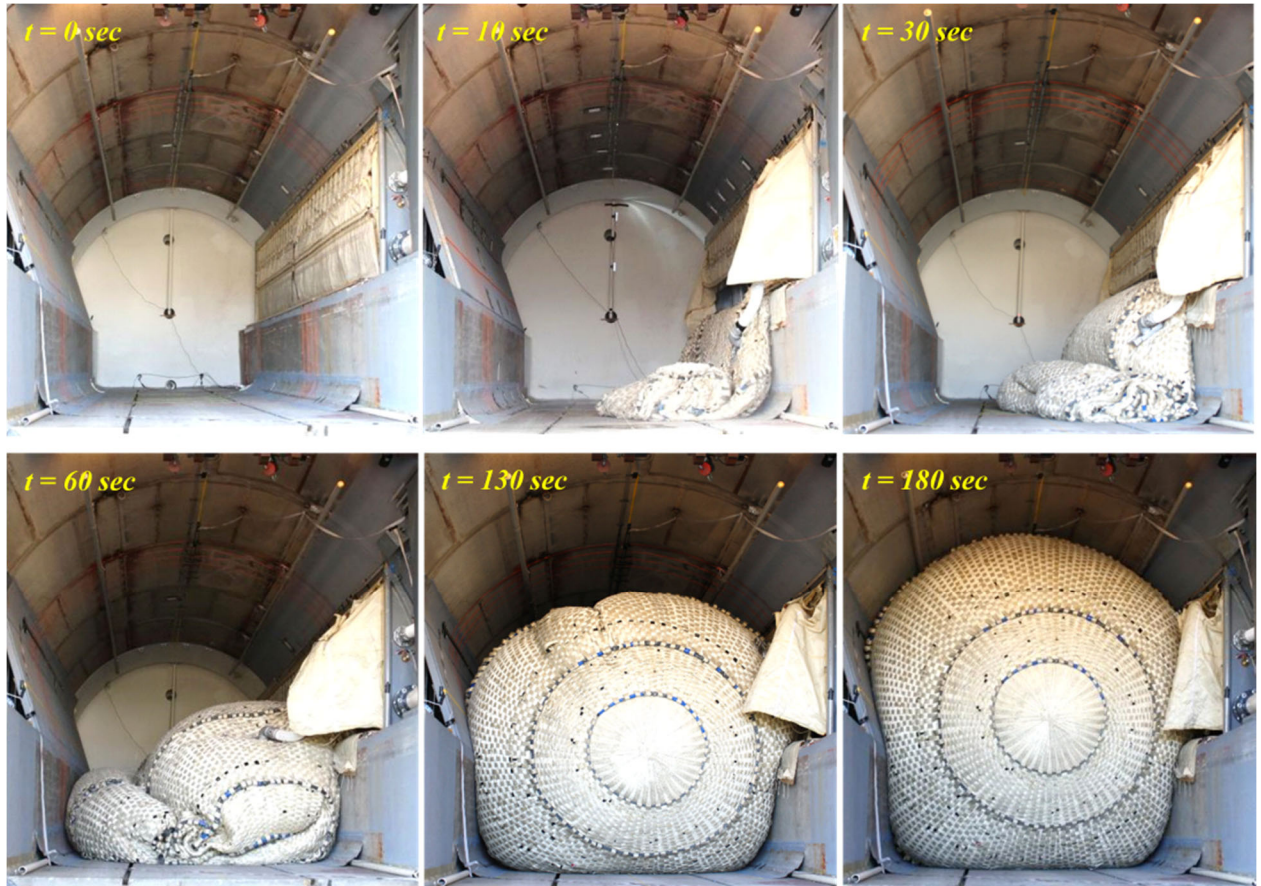


**Figure 2.** Example of full-scale experimental results for initial deployment and inflation [15-16].

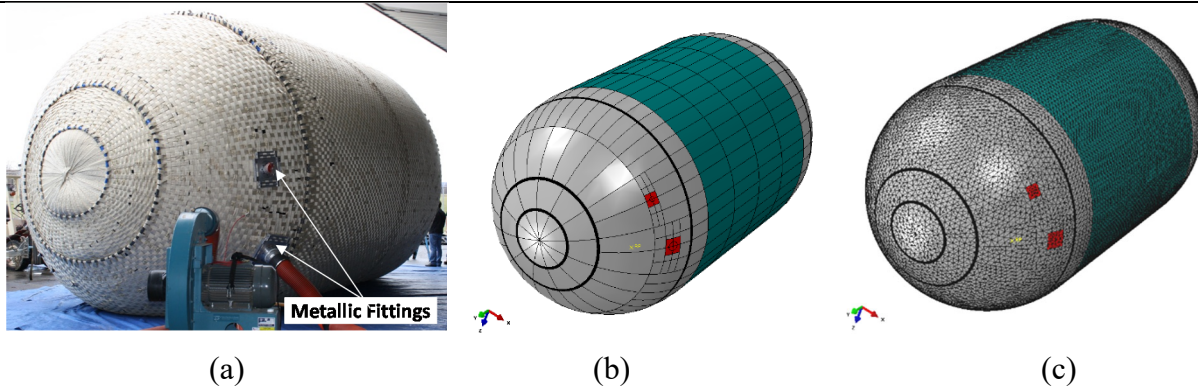


**Figure 3.** (a) Unconfined inflatable structure, actual full-scale prototype [15-16]; (b) Initial geometry with auxiliary partitions; (c) Final meshed configuration.

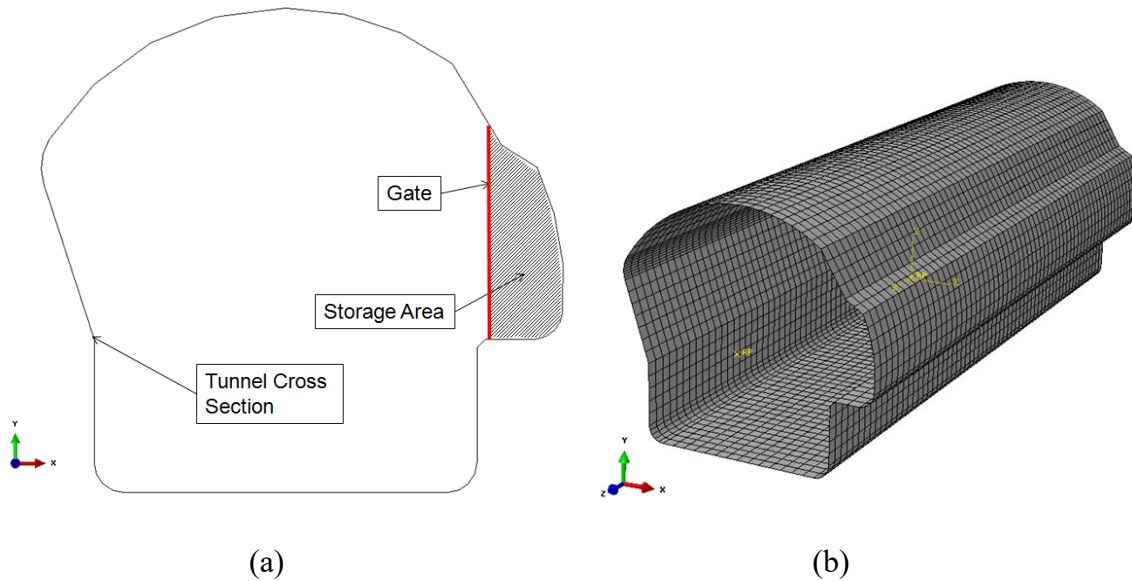


**Figure 4.** (a) Tunnel cross-section: Typical profile prepared for receiving a folded inflatable plug; (b) 3D meshed configuration used in the FE models.

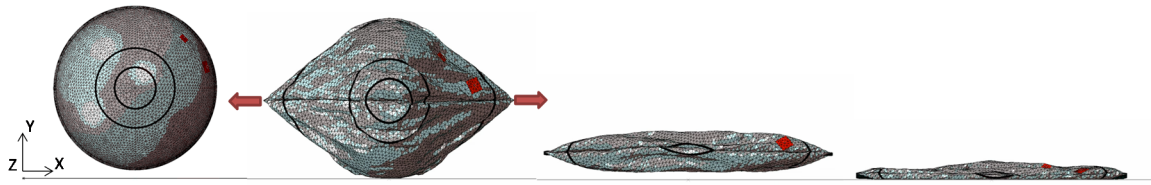


**Figure 5.** Sequence of deflation, flattening and grounding in preparation for folding.

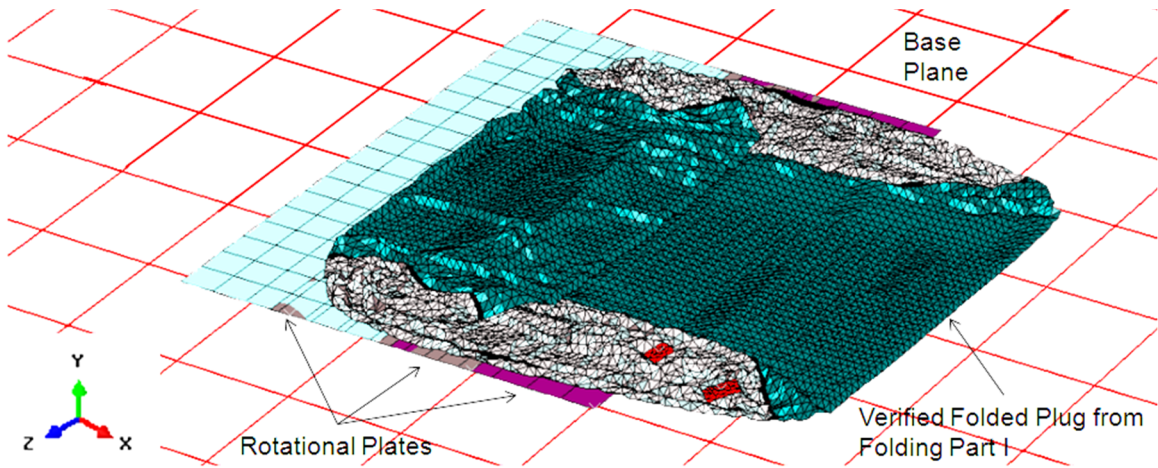


**Figure 6.** Flattened inflatable structure at the start of the folding process.

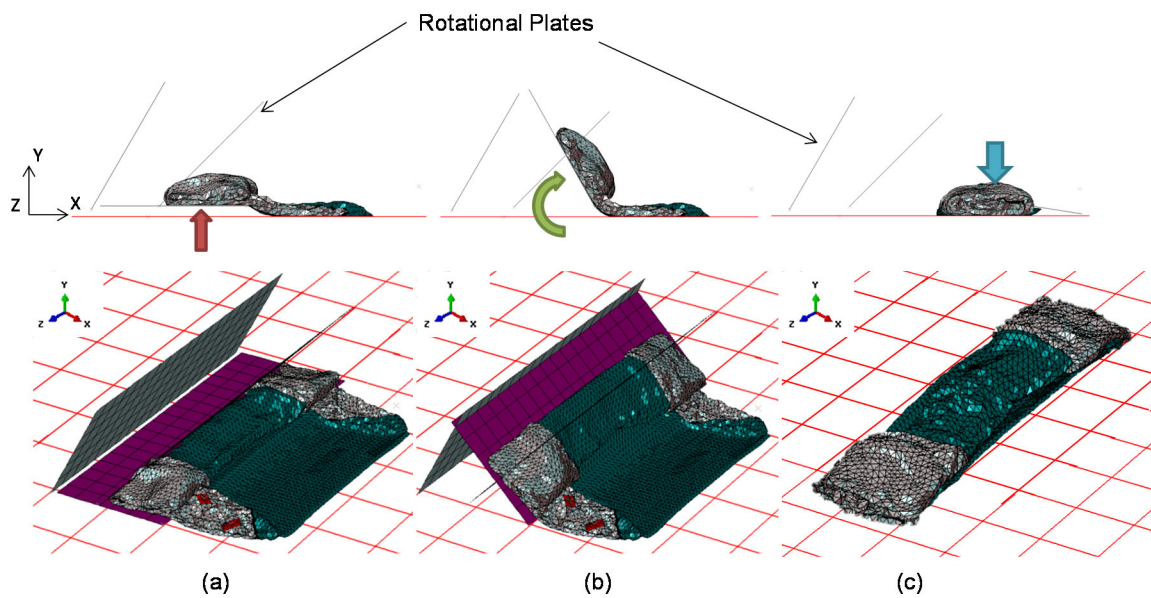


**Figure 7.** Folding sequence: (a) Vertical lifting; (b) Partial rotation; (c) Action of vertical gravity force. This sequence was repeated three times.

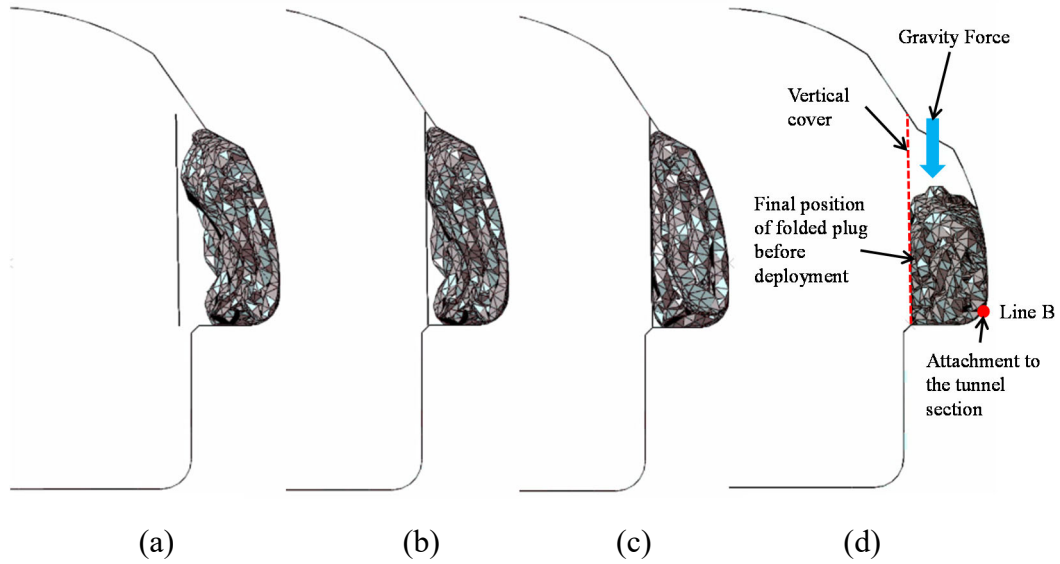


Figure 8. Placement of folded plug in storage area.

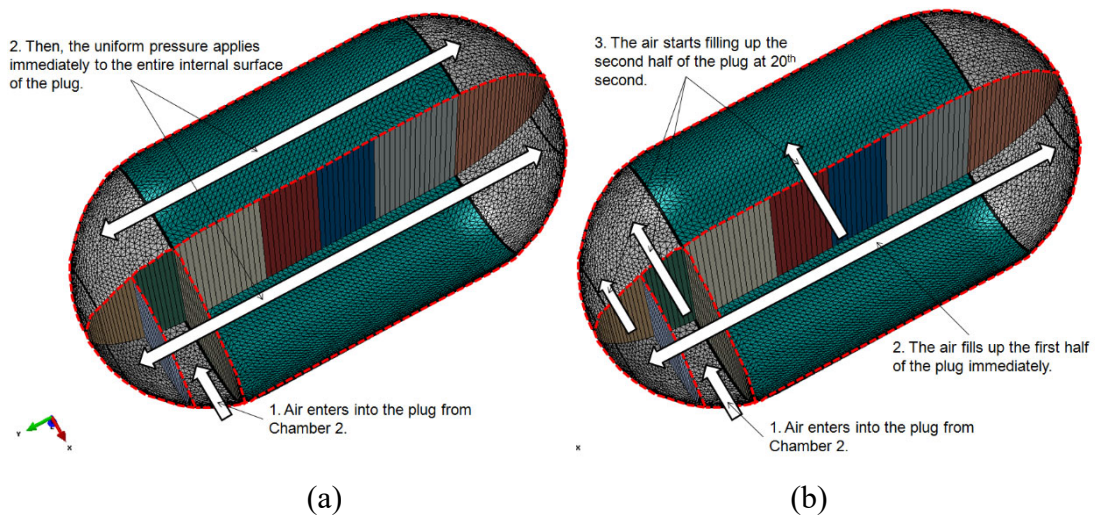
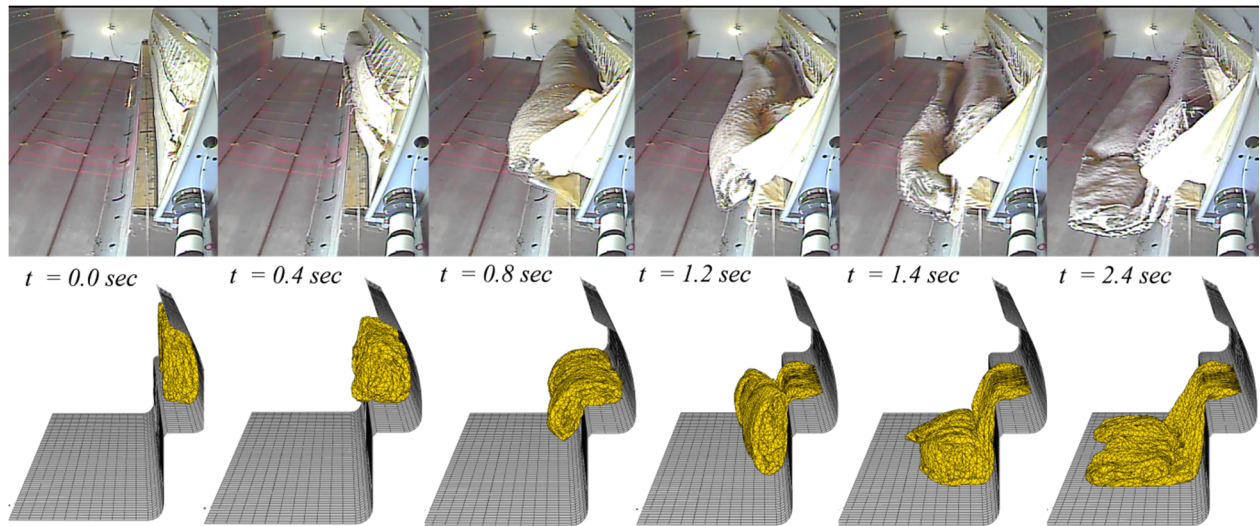
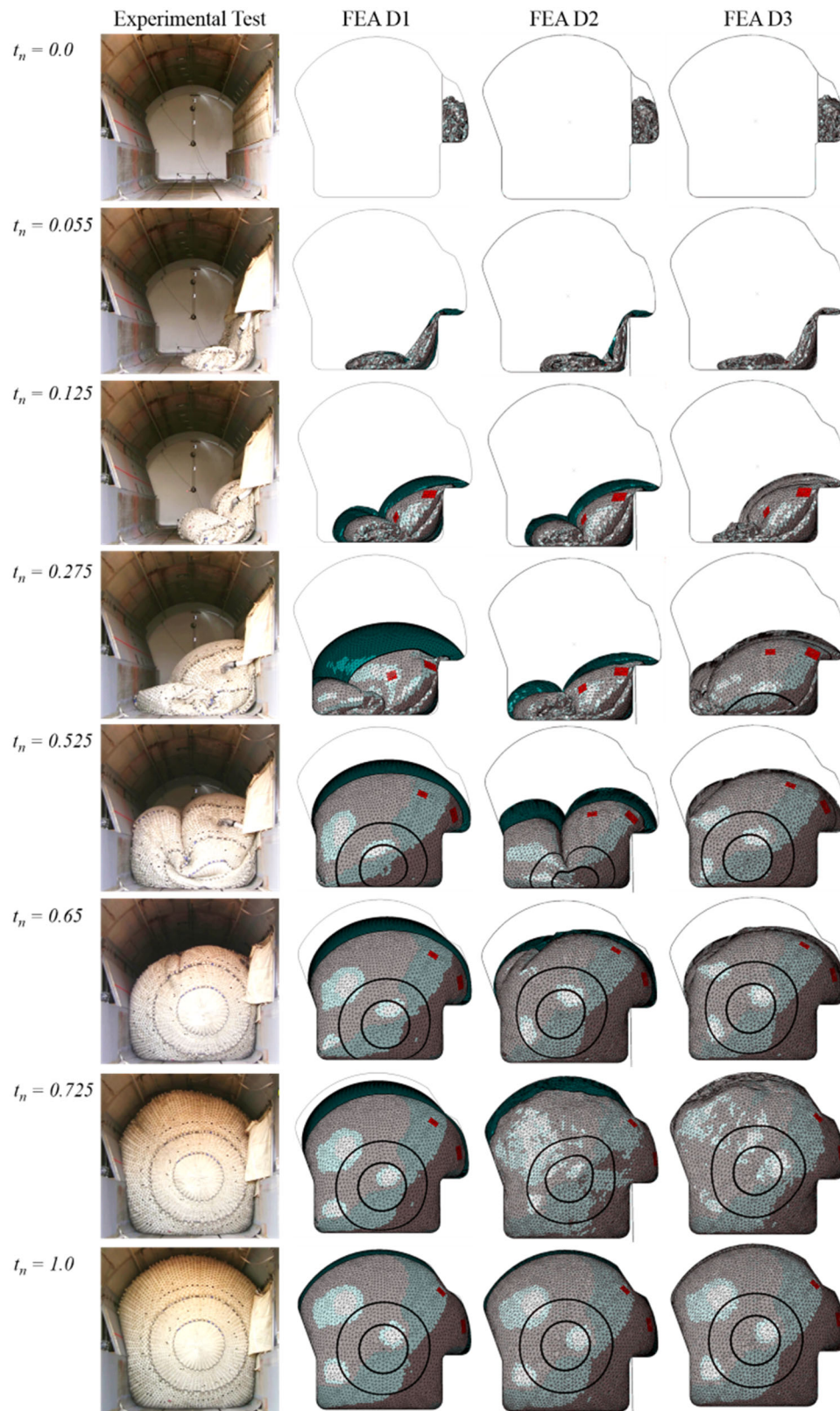


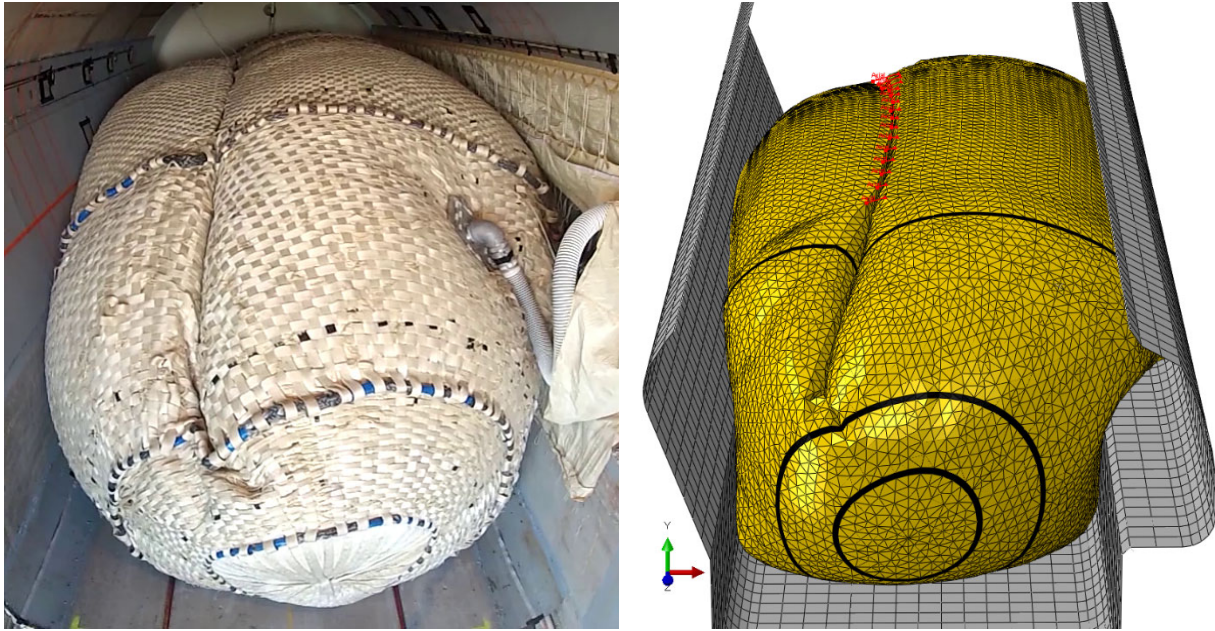
Figure 9. Position of chamber walls and flow direction within the inflatable plug; (a) Unguided airflow; (b) Guided airflow.



**Figure 10.** Sequence of initial unfolding of folded plug by own weight. Top, experiments [15-16]; Bottom, FE results (vertical cover removed for clarity).



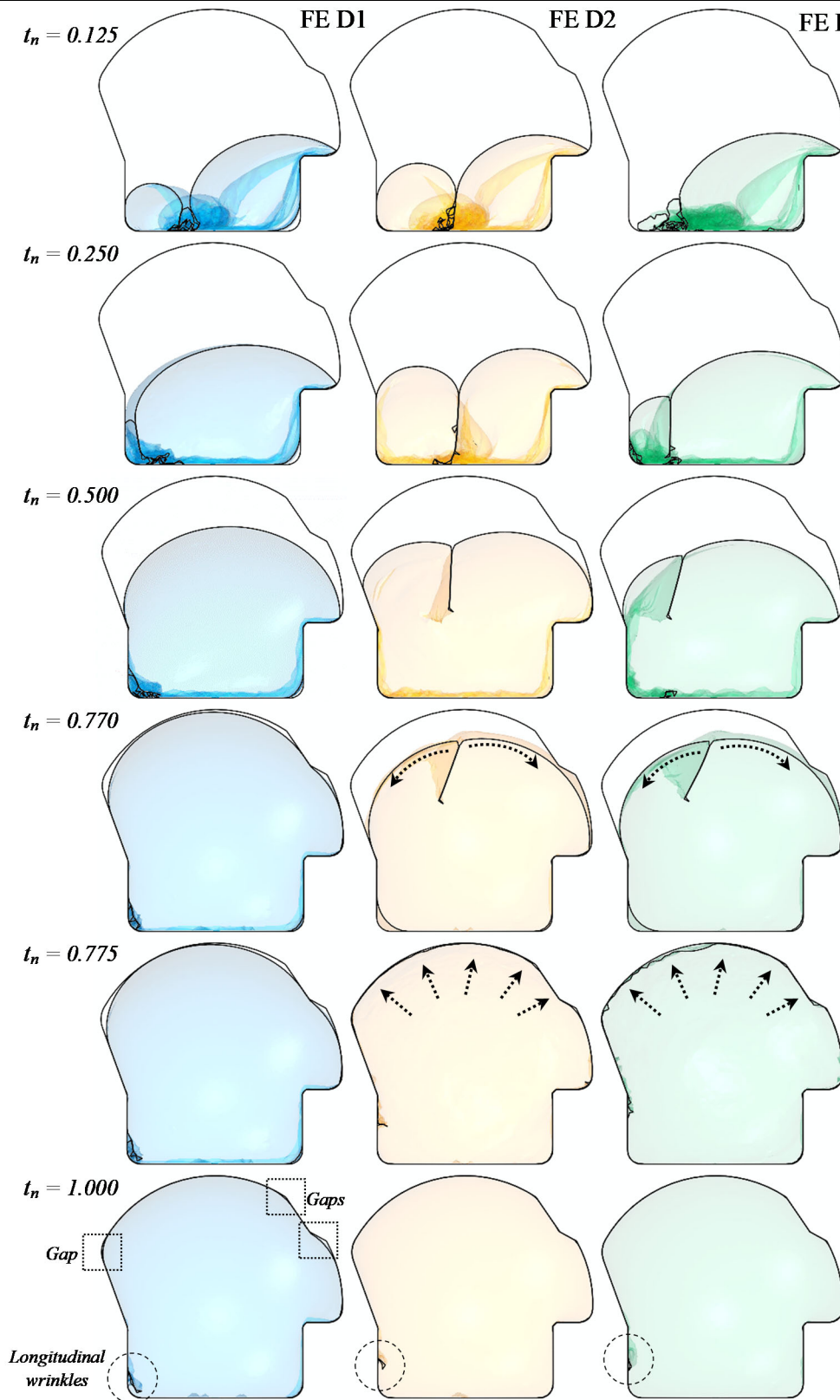
**Figure 11.** Experimental results [15-16] vs. FE simulation results (total analysis time  $t_T = 200$  sec; normalized time  $t_n = t / t_T$ ).



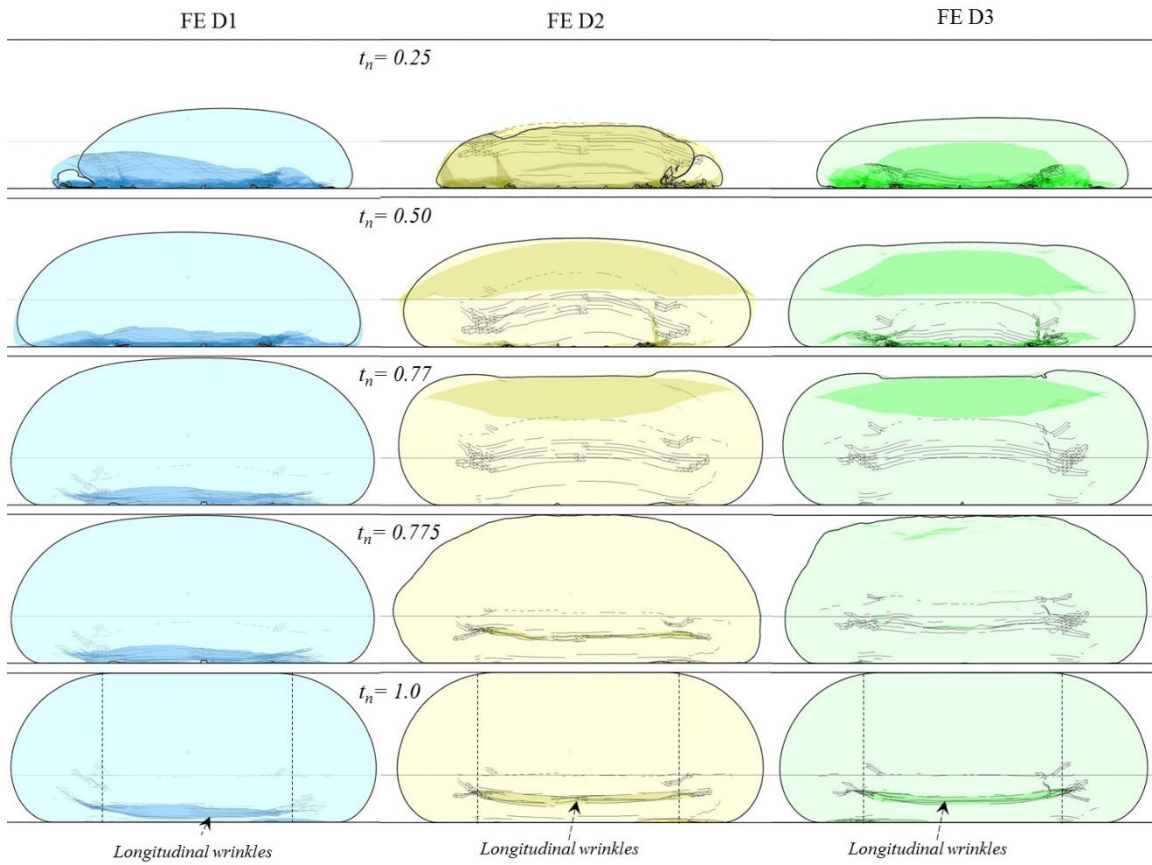
(a)

(b)

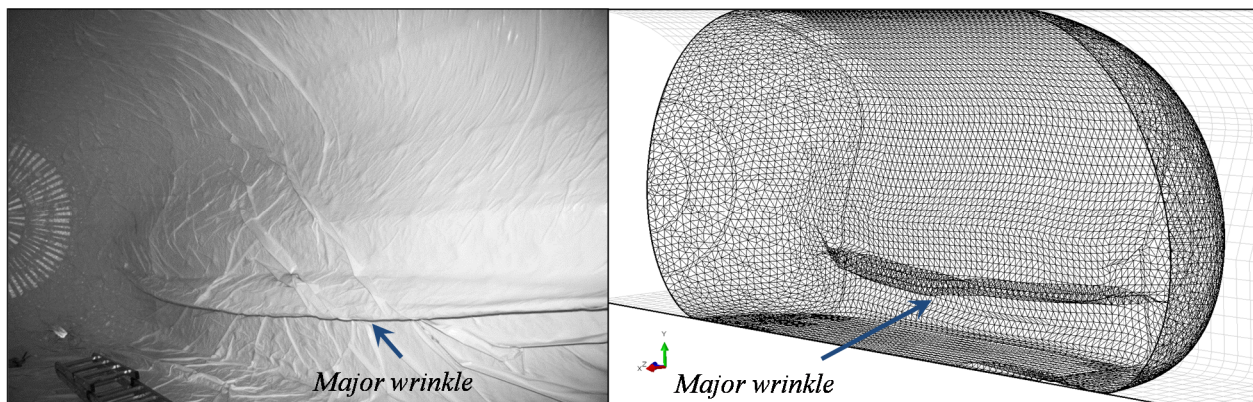
**Figure 12.** Detail of membrane restraining during inflation at  $t_n = 0.525$ . (a) Experimental results [15-16]; (b) FE simulation for model D2.



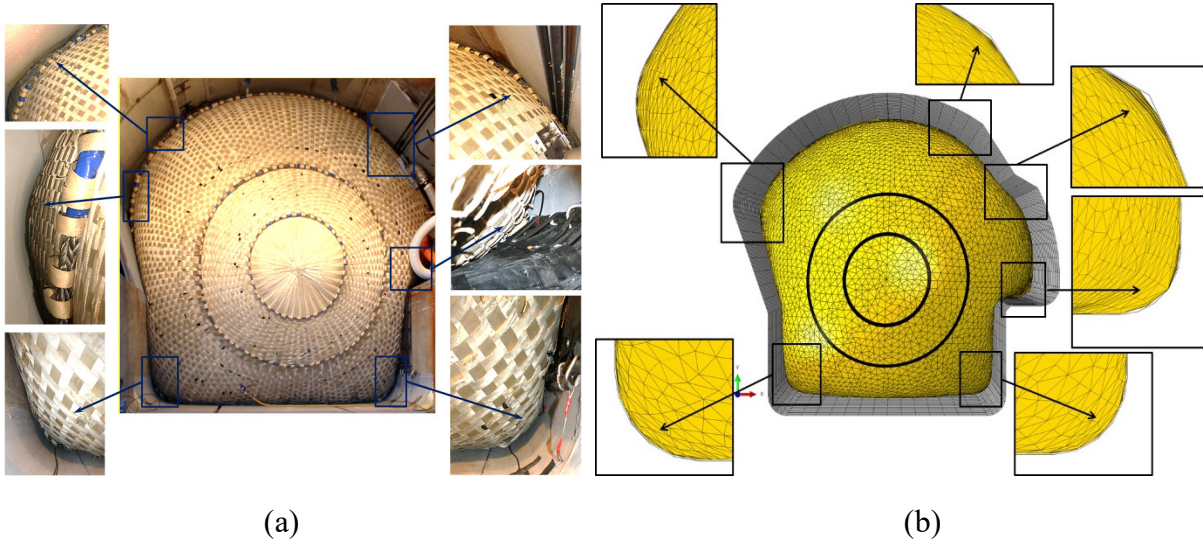
**Figure 13.** FE simulations: Transversal cross-sections of inflation models D1, D2 and D3 (total analysis time  $t_T = 200$  sec; normalized time  $t_n = t / t_T$ ).



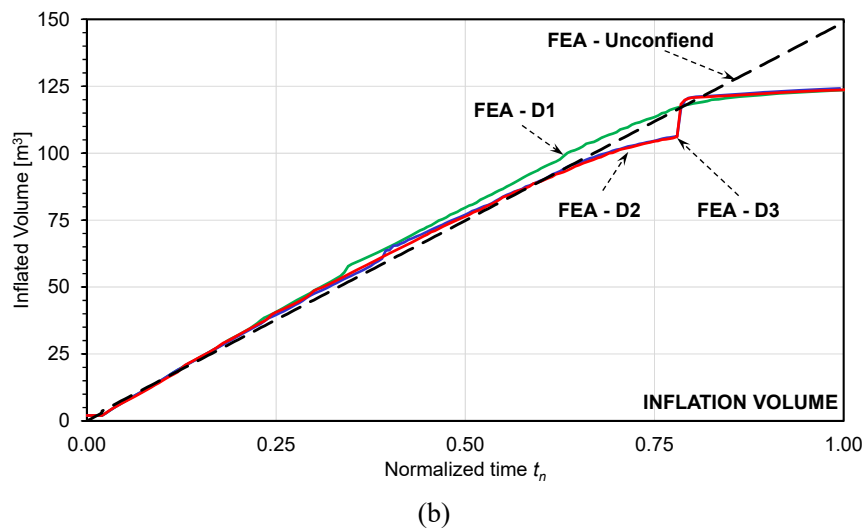
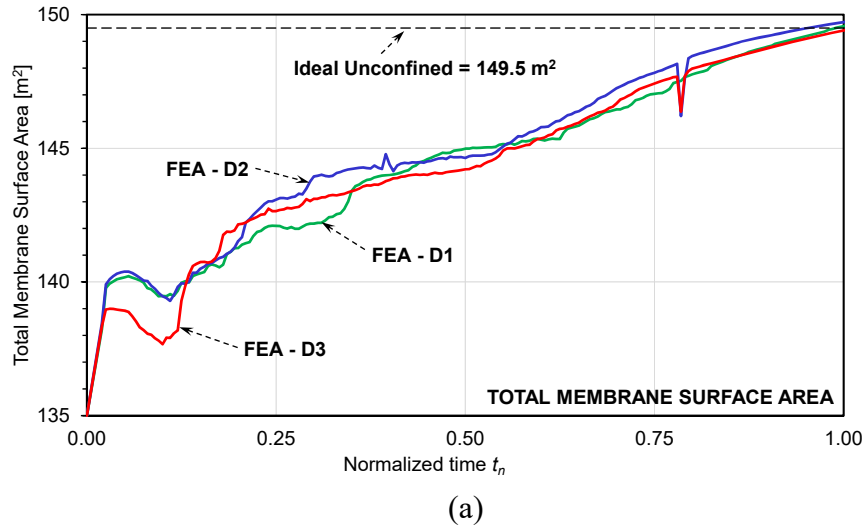
**Figure 14.** FE simulations: Longitudinal cross-sections of inflation models D1, D2 and D3 (total analysis time  $t_T = 200$  sec; normalized time  $t_n = t / t_T$ ).

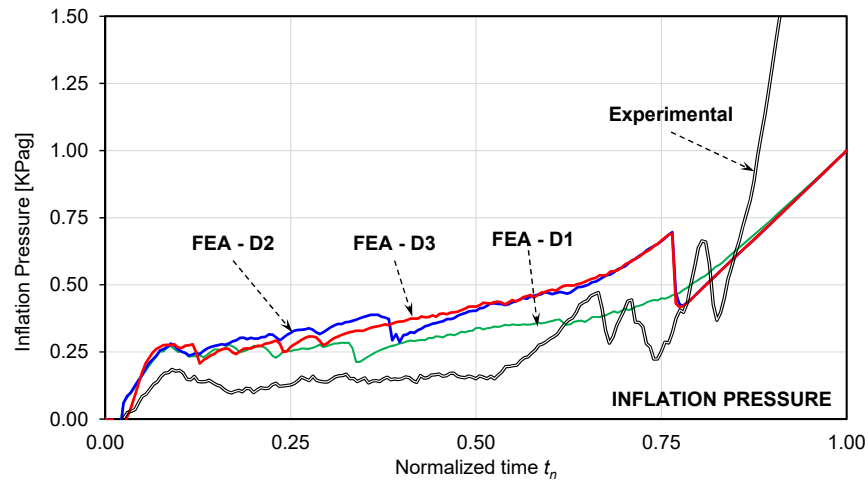


**Figure 15.** Detail of longitudinal wrinkles: (a) experimentally [15-16]; (b) FE simulation, model D3.

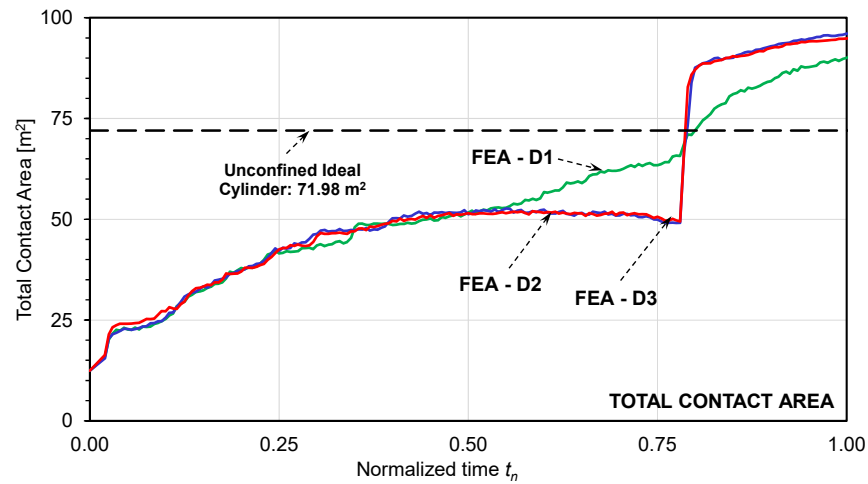


**Figure 16:** Evaluation of local conformity: (a) Experimental results [15-16]; (b) FE simulation results, model D3.





(c)



(d)

**Figure 17.** FE results. (a) Total membrane surface area; (b) Inflation volume; (c) Inflation pressure; (d) Total membrane contact area (total analysis time  $t_T=200$  sec; normalized time  $t_n=t/t_T$ ).

**Table 1.** Membrane area and total contact area at the end of inflation ( $t_n = 1.0$ ).

Parameter / Model	D1	D2	D3
Theoretical Total Membrane Area (m <sup>2</sup> )	149.50	149.50	148.50
Model Total Membrane Area (m <sup>2</sup> )	149.70	149.79	149.52
Difference (%)	+0.13%	+0.20%	+0.01%
Unconfined Inflation Cylindrical Contact Area (m <sup>2</sup> )	71.98	71.98	71.98
Confined Inflation Simulation Contact Area (m <sup>2</sup> )	90.17	95.27	96.27
Contact Enhancement %	+25%	+32%	+34%
Gaps or Bridging Spots	3	0	0